

URTeC: 650**Fracture analysis before and after Hydraulic Fracturing in the Marcellus Shale using the Mohr-Coulomb failure criteria**

*Kaitlin Evans¹, Randy Toth¹, Tobi Ore¹, Jarrett Smith¹, Natalia Bannikova¹
Timothy Carr¹, Payam Kavousi Ghahfarokhi¹*

¹Department of Geology and Geography, West Virginia University, Morgantown, WV

Copyright 2019, Unconventional Resources Technology Conference (URTeC) DOI 10.15530/urtec-2019-650

This paper was prepared for presentation at the Unconventional Resources Technology Conference held in Denver, Colorado, USA, 22-24 July 2019.

The URTeC Technical Program Committee accepted this presentation on the basis of information contained in an abstract submitted by the author(s). The contents of this paper have not been reviewed by URTeC and URTeC does not warrant the accuracy, reliability, or timeliness of any information herein. All information is the responsibility of, and, is subject to corrections by the author(s). Any person or entity that relies on any information obtained from this paper does so at their own risk. The information herein does not necessarily reflect any position of URTeC. Any reproduction, distribution, or storage of any part of this paper by anyone other than the author without the written consent of URTeC is prohibited.

Abstract

Data obtained from the Marcellus Shale Energy and Environment Laboratory (MSEEL) project was used to understand how pre-existing fractures behave under elevated pore pressure. 1680 pre-existing fractures were identified along the lateral of the MIP-3H well. Image logs and 3D computer tomography (CT) scan of the cores was used for fracture location and most fractures were identified as calcite-filled and resistive. In addition, sonic scanner well logs provided minimum horizontal stresses for every few feet, and the pilot-hole density log provided the vertical stress at each point along the lateral. This collection of geologic and geomechanical data helped us to establish an anisotropic stress field with separate stress tensors for each stage. Twenty-eight stress tensors were constructed corresponding to twenty-eight completion stages within the MIP-3H well. The vertical stress component of the tensors was calculated by integrating MIP-3 pilot-hole density log to the average depth of each stage. The minimum horizontal stresses (Sh_{min}) were also calculated by averaging the recorded Sh_{min} readings in each stage. Maximum horizontal stress (Sh_{max}) was calculated by a third-party logging vendor by adding a 400 psi to the Sh_{min} values. The stress tensors were transformed into a geographic coordinate system along with the dip and strike of each fracture. The transformed coordinate system (North-East-Down) was used when applying Cauchy's Stress theorem to every singular fracture within each stage to calculate the normal and shear stress components on each fracture. A Mohr diagram was created for each stage with two failure criteria lines corresponding to μ (μ) values of 0.6 and 1.0. Fractures are displayed on the diagram using their calculated normal and shear stresses. The pore pressure increase found from the average treatment pressure for each stage was applied and whether natural fractures experienced tensile or shear failure was inspected. The objective is to understand if natural fractures experience shear failure or tensile failure during hydraulic fracturing and determine if there is a contrast in the response between resistive (calcite-filled) and conductive

fractures. It was observed that prior to hydraulic fracturing, resistive natural fractures are mechanically dead and are in the stable region of the Mohr diagrams. Results show that although the majority of the pre-existing fractures are identified as resistive and mineral-filled, they undergo tensile failure when pore pressure was increased during hydraulic fracturing.

Introduction

Unconventional oil and gas plays have become major producers globally and have transformed the United States energy sector. Unconventional shale wells have resulted in abundant natural gas energy for the U.S., and research by corporations such as MSEEL are working toward efficient hydraulic fracturing while minimally impacting the environment. The Marcellus Shale is one of the largest unconventional plays in the world and extends throughout much of the Appalachian basin (Figure 1a) (Wang and Carr, 2013). Because shale reservoirs have very little permeability, induced permeability is required to allow for hydrocarbon flow. Creating permeability within the source rock is one main concern when hydro-fracturing a mudstone formation. Carr et al. (2017) suggests that understanding the distribution and influence of these pre-existing fractures is vital when improving completions in a well. The idea that the majority of reservoir stimulation is through the reactivation of pre-existing fractures rather than the creation of new fractures is generally accepted and that those pre-existing fractures affect the stimulation process. It is essential that these fractures open when hydraulically stimulated because pre-existing fractures contribute considerably more to the creation of permeable pathways by fracture network than those induced during the fracture process. The reactivation of these pre-existing fractures is key to successful unconventional well production.

With sufficient data, it is possible to plot the fractures as points on a three-dimensional Mohr diagram (Zoback, 2010). The orientation of the maximum horizontal stress in this area was determined to be N57°E by analysis of microseismic trends. (Wilson and Sullivan, 2016; Wilson et al., 2018). S_{hmin} was assumed to be in the direction 90° off of S_{hmax} . The largest principal stress was found to be the vertical stress (S_v) and the state of the stress as normal faulting. The direction of the stresses was then used to create a tensor transformation in order to eliminate the shear stresses (Zoback, 2010). Using this information, the fractures were plotted on a Mohr diagram to observe the change in stress state.

Background

The data used in this work came from the Marcellus Shale Energy and Environmental Laboratory (MSEEL) project. MSEEL consists of a multidisciplinary and multi-institutional team in engineering, geosciences and environmental research (Carr et al., 2017). The purpose of this research is to identify the best practices for optimizing hydraulic fracture stimulation while minimizing environmental impacts of unconventional resource development (Carr et al., 2017). Multiple wells have been drilled and completed for the MSEEL project, but the focus of this research is on data collected from the MIP-3H well.

Viable production of unconventional, shale-gas reservoirs requires hydraulic stimulation of multiple stages. Completion of this well included stimulation of 28 stages within five sections: A, B, C, D, and E. Stimulation of the reservoir stage to stage included high pressure injection

URTeC 650

averaging 8500 psi. The length of each stage was around 200 feet with four to five clusters per stage.

The MIP-3H well was drilled with N36°W heading within a section of the Marcellus roughly 100m thick. The MIP-3H was drilled just above the Cherry Valley Limestone at the transition between the upper and lower section of the formation and targets the high gamma-ray and organic-rich zone (Wilson et al., 2018).

During the Acadian Orogeny, large volumes of deltaic sediments were deposited within the Acadian Foreland Basin. This delta complex is comprised of two primary delta systems: 1) The Catskill Delta of Middle to Late Devonian age and 2) The Price-Rockwell Delta of Late Devonian to Early Mississippian age (Lash et al., 2011). The foreland basin-delta complex sedimentary wedges are responsible for the high volume of sediment influx into the Appalachian Basin (Lash et al., 2011). Relief caused by uplifting episodes acted as the sediment source feeding the delta systems. Clastic particles comprising the Marcellus Shale were sourced from the Catskill Delta (Lash et al., 2011). Rapid subsidence in the region resulted in a transgressive sequence that ultimately deposited the black shales of the Marcellus. These black shales were formed in the relatively deep, anoxic bottom water conditions of the epeiric sea parallel to the mountain chain (Chen et al., 2017). Radiometric age dating of the Marcellus Shale places the formation in the Middle Devonian at approximately 384 Ma (Chen et al., 2017).

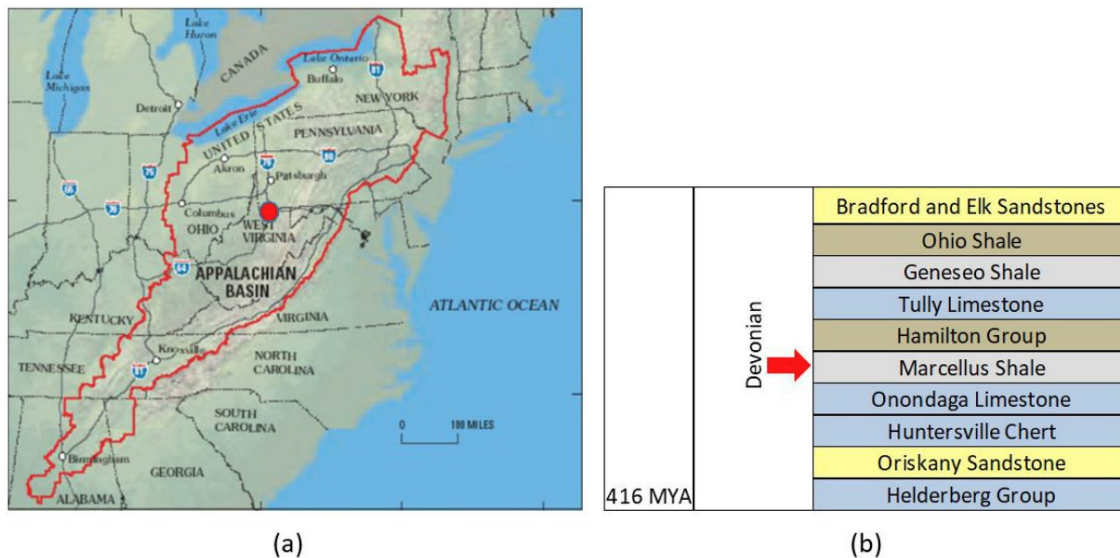


Figure 1 extent of the Appalachian Basin and the location of the MIP-3H well (a) along with the stratigraphic position of the Marcellus (b) adapted from (Bhattacharya, et al. 2019).

Two major natural fracture sets, J1 and J2, have been identified within the Marcellus (Engelder and Lash, 2009). Folding of the J1 set and bedding planes show that the J1 set formed early and most likely in response to high fluid pressure from the thermal maturation of organic material

URTeC 650

(Engelder and Lash, 2009). The J2 joint set may have formed in response to the formation of the fold and thrust belts that make up the Appalachian Valley and Ridge province (Engelder and Lash, 2009). Several subsurface studies have been completed in the area showing a N80°E set of fractures that corresponds with the J1 set and a N64°W set with an orientation similar to the J2 set (Engelder and Lash, 2009; Evans, 1980; Wilson et al., 2018).

Methodology

Azimuth values of pre-existing fractures within each stage were recorded using wireline image logs, as well as the P32 fracture intensity. This is the fracture area per unit volume.

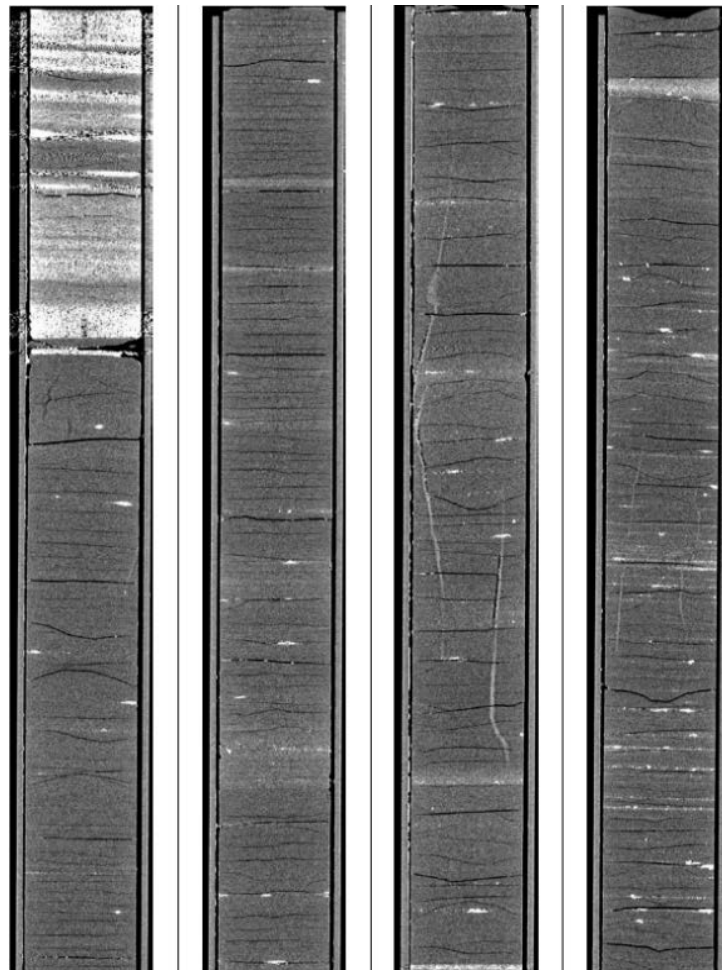


Figure 2 Calcite-filled fractures viewed through CT scan.

The corresponding pole locations were placed into stereonet associated with each stage. This is viewed in **Figure 3** and allows for a better view of the orientation of fractures.

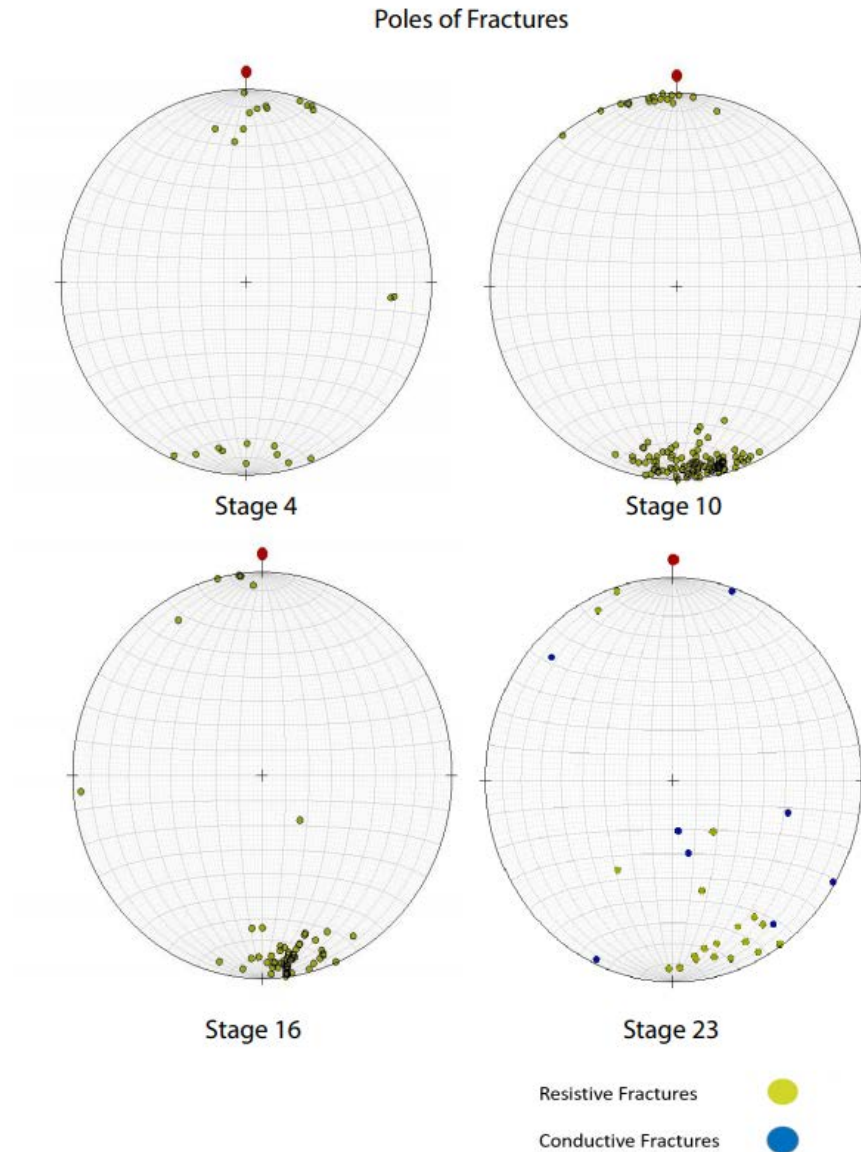


Figure 3 Generated stereonets displaying pole locations of corresponding fracture azimuth values.

Over 1600 natural fractures were identified along the length of the MIP-3H well using image logs (Wilson et al., 2018). Of these pre-existing fractures, 1078 were included within stage locations. Fractures were described as either conductive or resistive (mineral-filled). The resistive fractures ($n = 1068$) are more abundant than the conductive fractures ($n = 10$). Most of the conductive fractures were clustered in stage 23 (Figure 2) with an average trend of N72°E. Fractures were classified as resistive or conductive based on whether the fractures were mineral-filled or not respectively.

When performing the Mohr circle analysis on these pre-existing fractures, the average treatment pressure of each individual stage was applied. The overall average treatment pressure for the stages

URTeC 650

was 8,502 psi. Stage and treatment pressure data were obtained from Northeast Natural Energy's stimulation summary report on the MIP-3H well.

The stress state of the area was based on previous studies in the area. Wilson and Sullivan (2016) used microseismic event trends along with the Mohr-Coulomb failure criteria to estimate the orientation of the maximum horizontal stress in the study area. S_{max} of the local area has an orientation of N57°E this was determined using micro-seismic event trends (Wilson and Sullivan, 2016). This estimation was completed by orienting S_{max} in the direction where the fewest micro-seismic events fell below the failure envelope (Wilson and Sullivan, 2016).

Stress is defined as a force acting on a specified area. This stress can be described using a second-rank tensor with nine components as

Eq. 1:

$$S = \begin{bmatrix} S_{11} & S_{12} & S_{13} \\ S_{21} & S_{22} & S_{23} \\ S_{31} & S_{32} & S_{33} \end{bmatrix}$$

where the subscripts of the individual stress components refer to the direction of the force acting on a given face of the infinitesimal cube. Since the cube is not rotating, torque is zero. Therefore, the order of the subscripts will be unimportant as $S_{12} = S_{21}$, $S_{13} = S_{31}$ and $S_{23} = S_{32}$. The principal normal stress is represented by

Eq. 2:

$$S = \begin{bmatrix} S_1 & 0 & 0 \\ 0 & S_2 & 0 \\ 0 & 0 & S_3 \end{bmatrix}$$

This stress can be expressed in a geographical coordinate system using the transform

Eq. 3:

$$S_g = R'_1 S R_1$$

where

Eq. 4:

$$R_1 = \begin{bmatrix} \cos \alpha \cos \beta & \sin \alpha \cos \beta & -\sin \beta \\ \cos \alpha \sin \beta \sin \gamma - \sin \alpha \cos \gamma & \sin \alpha \sin \beta \sin \gamma + \cos \alpha \cos \gamma & \cos \beta \sin \gamma \\ \cos \alpha \sin \beta \cos \gamma + \sin \alpha \sin \gamma & \sin \alpha \sin \beta \cos \gamma - \cos \alpha \sin \gamma & \cos \beta \cos \gamma \end{bmatrix}$$

α , β , and γ are the rotation angles that define the stress coordinate system in terms of geographic coordinates.

The geographic coordinate system created using stress tensors and fracture orientation discussed above were used in the application of Cauchy's Stress Theorem. This coordinate system (North-East-Down) was used when applying the theorem to every fracture at each stage to calculate normal and shear stress components. Cauchy's Stress Theorem is shown in the Eq.5 where \vec{T} represents the vector value of the traction on a plane with respect to the normal vector \vec{n} , and $\vec{\sigma}^T$ denotes the transposed stress tensor.

Eq. 5:

$$\vec{T} = \vec{\sigma}^T \cdot \vec{n}$$

This traction vector \vec{T} is the value limiting the ratio of force over a surface, while n indicates the normal to that surface. The normal vector can be used to determine the traction vector that is acting on the plane. In this case, the planes being analyzed are the pre-existing fractures within the MIP-3H well. The transposed matrix (σ^T), Cauchy's Stress Tensor, in the formula above represents the stress acting on the surface of the fracture. This matrix is written below where "e" represents the unit vectors on the coordinate system.

Eq. 6:

$$\sigma = \begin{bmatrix} T_{X_1}^{(e1)} & T_{X_2}^{(e1)} & T_{X_3}^{(e1)} \\ T_{X_1}^{(e2)} & T_{X_2}^{(e2)} & T_{X_3}^{(e2)} \\ T_{X_1}^{(e3)} & T_{X_2}^{(e3)} & T_{X_3}^{(e3)} \end{bmatrix}$$

Failure of pre-existing fractures was identified by applying the stresses on each fracture in a Mohr diagram. A Mohr diagram was created for each individual stage and the accompanying fractures. For a fracture to undergo tensile failure, the strength or resistance of the fracture must be overcome (Zoback, 2010). Once the fracture starts to grow in length and exceeds several tens of cm, only a small amount of pressure above the minimum horizontal stress is required to extend those fractures (Zoback, 2010).

Results

Existing research on fracture activation in the subsurface combined with fracture failure data discussed here shows that all fractures, healed and open, are activated during hydraulic fracturing. Using data obtained from the MSEEL project, fracture location was plotted onto a three-dimensional Mohr diagram for each of the stages in the MIP-3H well. The stress tensors from each stage along with the strike and dip of each pre-existing fracture was used to plot the data points.

Figure 4 shows the graphical representation of the fracture in the four stages viewed in this paper. The diagrams show the stress states before and during the frac. The right circle shows the stress state before the frac with natural pore pressure applied. The circle on the left side of the graph

URTeC 650

shows the stress state with treatment pressure applied. During hydraulic fracturing the fractures enter the tensile failure regime. Research by Kavousi et al. 2017, showed that fractures within the core of the MIP-3H failed during tensile testing.

Three principal stresses (S_v , S_{hmax} , and S_{hmin}) were determined based on geologic information from the Marcellus Shale formation surrounding the study area. Based on the results of this research, it is concluded that all pre-existing fractures, mineral-filled and open, were activated during the fracture process.

Discussion

Research conducted on the tensile failure of fractures within the MIP-3H core lead to similar results as discussed above. These pre-existing fractures failed even when calcite-filled. The analysis conducted showed a connection between the P32 fracture intensity and the distribution of fiber optic hDVS energy. Stages with more pre-existing fractures vibrated less than those with a low P32. This showed the connection between fracture intensity and hydraulic fracturing efficiency. The lower the P32, the more energy was required to induce fractures. A higher P32 resulted in less hDVS required, because the rock was more easily broken. Because all pre-existing fractures experienced tensile failure during hydraulic fracturing, the calcite fill has very little to no effect on hydraulic fracturing efficiency (Kavousi, et al., 2017).

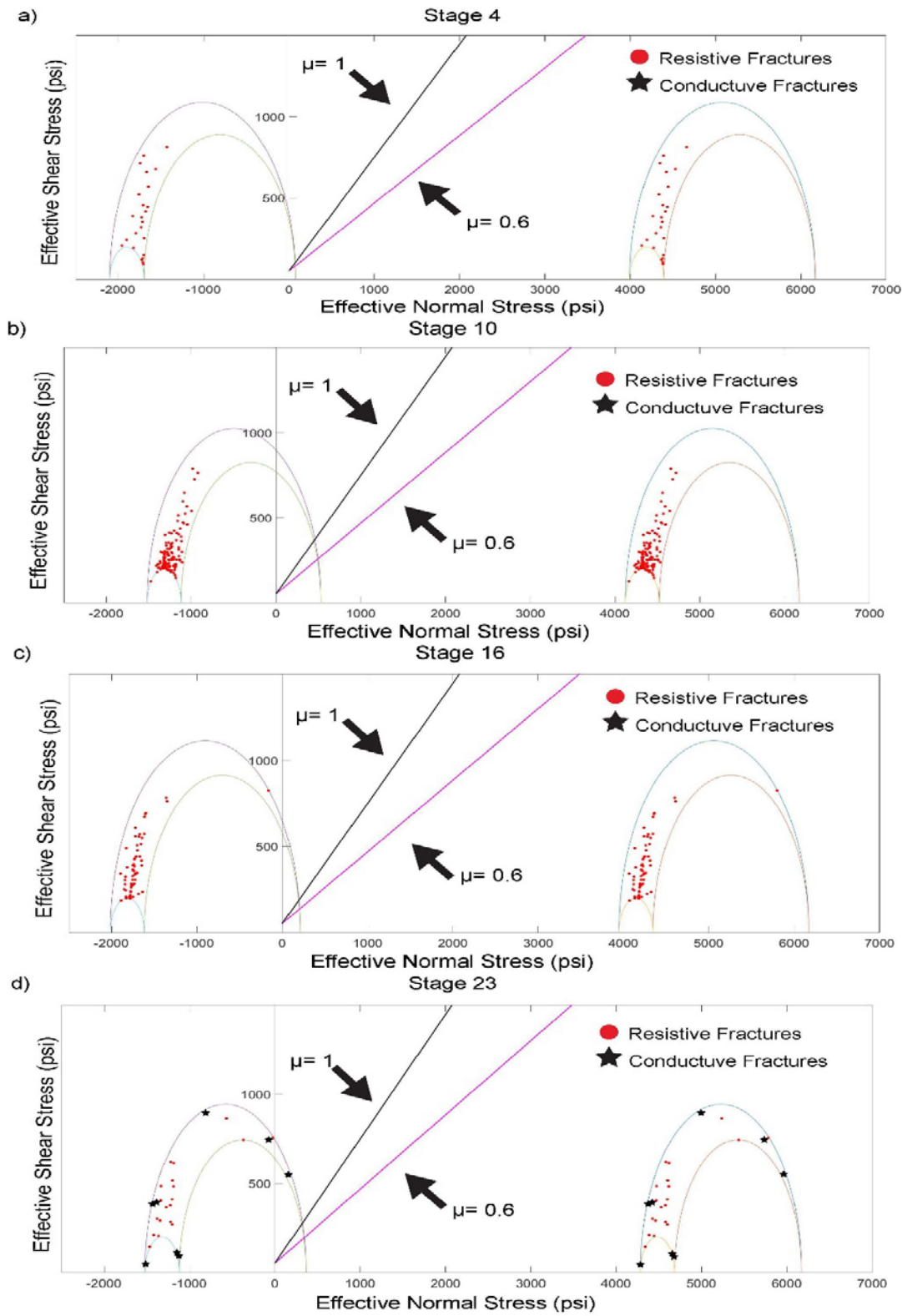


Figure 3 Fractures in four stages of the MIP-3H well plotted on a Mohr diagram. Conductive fractures in all stages show the same trends in the Mohr Circle. Conductive fractures shown as stars are located along the edge of the circle.

Conclusions

Wireline image logs were used to identify natural fractures within the lateral portion of the well. The contrast between calcite, which fills most fractures within the Marcellus, and shale allowed for easy identification of these fractures. Over 1600 of the pre-existing fractures present were resistive, calcite-filled, as well as a few conductive, or open, fractures. The behavior of pre-existing fractures when exposed to high pressures during hydraulic stimulation may lead to a better understanding of variables impacting stimulation efficiency and overall recovery efficiency of unconventional, shale-gas wells.

Natural fractures make up much of the permeability that allows for gas flow in unconventional shale wells, so it is key that these fractures open during stimulation of the reservoir. Data sourced from a Marcellus Shale well in northern West Virginia, U.S.A allowed for failure analysis of naturally-occurring fractures under regional geologic stresses as pressure is introduced during stimulation. Over 1600 fractures were plotted on Mohr diagrams representing pressures before and during hydraulic stimulation for each stage using the stress values of the area and treatment pressures. The analysis showed that all fractures, whether resistive or conductive, underwent tensile failure. This shows that all fractures are contributing to the permeability of the reservoir after the hydraulic fracturing process.

Acknowledgements

This research is funded through the U.S.DOE National Energy Technology Lab part of their Marcellus Shale Energy and Environmental Laboratory (MSEEL) (DOE Award No.: DE-FE0024297). Matlab software was used for much of the analysis. A special thanks to Northeast Natural Energy, Schlumberger, WVU and all other companies and organizations involved with the MSEEL project.

References

- Bhattacharya, S., Kavousi, P., Carr, T., Pantaleone, S., 2019, Application of predictive data analytics to model daily hydrocarbon production using petrophysical, geochemical, fiber-optic, completions, and surface data: A case study from the Marcellus Shale, North America: *Journal of Petroleum Science and Engineering*, **176**, 702-715
- Chen, Ruiqian, and Shikha Sharma. "Linking the Acadian Orogeny with organic-rich black shale deposition: Evidence from the Marcellus Shale." *Marine and Petroleum Geology* 79 (2017): 149-158.
- Engelder, T., Lash, G.G., 2009, Joint sets that enhance production from Middle and Upper Devonian gas shales of the Appalachian Basin: *AAPG Bulletin*, **93**, 857-889, doi:10.1306/03230908032

- Lash G. G., Engelder T. 2011. Thickness trends and sequence stratigraphy of the Middle Devonian Marcellus Formation, Appalachian Basin: Implications for Acadian foreland basin evolution. *AAPG bulletin*, 95(1), 61-103.
- Kavousi, Payam, Timothy Carr, Thomas Wilson, Shohreh Amini, Collin Wilson, Mandy Thomas, Keith MacPhail et al. "Correlating distributed acoustic sensing (DAS) to natural fracture intensity for the Marcellus Shale." In *SEG Technical Program Expanded Abstracts 2017*, pp. 5386-5390. Society of Exploration Geophysicists, 2017
- Wang G., Carr T.R., 2013. Organic-rich Marcellus Shale lithofacies modeling and distribution pattern analysis in the Appalachian basin. *AAPG bulletin*, 97(12), 2173-2205
- Wang G., Carr T.R., 2012. Methodology of organic-rich shale lithofacies identification and prediction: A case study from Marcellus Shale in the Appalachian Basin. *Computers and Geoscience*, 49, 151-163
- Wilson T.H., Carr T.R., Carney B J., Yates M., MacPhail K., Morales A., Costello I., Hewitt J., Jordan E., Uschner N., Thomas M., Akin S., Magbagbeola O., Johansen A., Hogarth L., Anitowoshe O., Naseem K., 2018, Marcellus Shale model stimulation tests and microseismic response yield insights into mechanical properties and the reservoir discrete fracture network: *Interpretation*, 6(2), 1-50, doi:10.1190/INT-2016-0199.1
- Wilson T.H., Sullivan P., 2016, Microseismic energy density and event trend constraints on model DFN development for hydraulically fractured reservoirs: Marcellus shale, south western Pennsylvania, U.S.A.: 86th Annual International Meeting, SEG, Expanded Abstracts, 3093-3097, doi: 10.1190/segam2016-13528380.1.
- Zoback, M. D., 2010, Reservoir geomechanics: Cambridge University Press.
- U.S EIA, 2019. Natural Gas. *Annual Energy Outlook 2019 with Projections to 2050*. 69-86
- Timothy R Carr, Thomas H. Wilson, Payam Kavousi, Shohreh Amini, Shikha Sharma, West Virginia University: Jay Hewitt, Ian Costello, B. J. Carney, Emily Jordan, Northeast Natural Energy LLC: Malcolm Yates, Keith MacPhail, Natalie Uschner, Mandy Thomas, Si Akin, Oluwaseun Magbagbeola, Adrian Morales, Asbjorn Johansen, Leah Hogarth, Olatunbosun Anifowoshe, Kashif Naseem, Schlumberger: Richard Hammack, Abhash Kumar, Erich Zorn, Robert Vagnetti, and Dustin Crandall, National Energy Technology Laboratory, US Department of Energy., 2017, Insights from the Marcellus Shale Energy and Environment Laboratory (MSEEL), Unconventional Resources Technology Conference, Austin, July 2017 , DOI 10.15530-urtec-2017-2670437